Real-Time PEV Charging/Discharging Coordination in Smart Distribution Systems

M. F. Shaaban, *Student Member, IEEE,* Muhammad Ismail, *Student Member, IEEE,*
E. F. El-Saadany, *Senior Member, IEEE,* and Weihua Zhuang, *Fellow, IEEE*

***Abstract*—This paper proposes a novel online coordination method for the charging of plug-in electric vehicles (PEVs) in smart distribution networks. The goal of the proposed method is to optimally charge the PEVs in order to maximize the PEV owners' satisfaction and to minimize system operating costs without violating power system constraints. Unlike the solutions reported in the literature, the proposed charging architecture guarantees the feasibility of the charging decisions by means of a novel prediction unit that can forecast future PEVs power demand and through an innovative two-stage optimization unit that ensures effective charging coordination. Coordinated PEV discharging also enables improved utilization of power system resources. Simulation results for a typical distribution network are provided as a demonstration of the effectiveness of the proposed architecture.**

***Index Terms*—Distribution systems, energy management, electric vehicle, smart parking lot, $M/G/\infty$ queue.**

I. Introduction

ECONOMIC, and environmental concerns have led to a recent increase in interest in low or zero emission vehicles. One promising type of low emission vehicle is the plug-in electric vehicle (PEV), the development of which has been motivated by the recent growth of renewable energy sources and the almost universal availability of electric power systems. PEVs are now commercially available at a wide range of prices, and thousands of PEVs are operating in many countries around the world.

It has been shown that the PEV charging process, if not managed effectively, can entail potential risk to the electric power system, even with low PEV penetration [1], [2]. The risk is due primarily to the probability that PEVs will likely be clustered in specific geographical areas, resulting in significant stress on the local power distribution system. If not managed appropriately, the additional load imposed by high PEV penetration is expected to have severe consequences, such as increased power losses, phase imbalances, power quality problems, transformer degradation, and fuse blowouts [2]. The literature provides two categories of solutions that have been proposed in order to resolve these problems. The first involves uncoordinated PEV charging, which is possible either through upgrades to the power system infrastructure or through the deployment of distributed generation (DG) units to meet the excess power demand [3]. The second category targets coordinated PEV charging or charging/discharging, which relies on a two-way communication infrastructure under a smart grid paradigm [4]. Coordinated smart PEV charging and discharging is known to be overall more beneficial for electric grid operators and customers than uncoordinated operation [5].

A smart charging and discharging coordination architecture consists of three main units: a data collection and storage unit, a prediction unit, and an optimization unit [6]. The data collection and storage unit governs the collection of information related to current PEV power demands, the current state-of-charge (SOC) of PEV batteries, and the power demand of regular loads. In most cases, an aggregator is assumed to be in place to deal with PEV data collection and storage. The role of the aggregator is to collect information from the PEVs and send it to the grid operator, and to send charging/discharging decisions from the operator to the chargers. The prediction unit should provide accurate forecasts of future PEV power demands and regular loads in the power system. Based on this information, the optimization unit should then make optimal coordinated charging and discharging decisions that guarantee service reliability, maximize operator profit, satisfy system constraints, and meet customer power demands.

One limitation of the solutions proposed in the literature is that most fail to address coordinated PEV charging and discharging decisions that are based on real-time measurements from the grid. As a result, the effect of current and future PEV charging and discharging decisions on the power grid is not considered. While some studies involve coordinated decisions based on PEV load forecast data, not many details are available with respect to the actual performance of the PEV load forecast, and perfect PEV load forecast data are usually assumed. The system response to short-term fluctuations in the PEV load is therefore not examined. As well, in most cases, the problem formulation fails to include consideration of electric power grid constraints and customer power demands. Customer satisfaction and the feasibility of the decisions are hence not guaranteed.

This paper presents a real-time coordinated charging and discharging architecture for a smart grid. The proposed architecture is capable of dynamically managing PEV charging and discharging in commercial, industrial, or residential parking lots. The research contributions can be summarized as follows:

- A novel real-time smart coordinated charging and discharging architecture: The architecture consists of two new prediction and optimization units, which can improve power system resource utilization.
- An innovative parking lot prediction unit based on an $M/G/\infty$ queuing model: The input to the prediction

The authors are with the Department of Electrical and Computer Engineering, University of Waterloo, Waterloo, Canada, e-mail:{m2farouk, m6ismail, ehab, wzhuang}@uwaterloo.ca.

unit includes current information about the PEVs in the parking lot along with the PEV arrival and departure rates (based on historical data). The unit then outputs, with a small probability of prediction error, a predicted number of PEVs that will be simultaneously present in the parking lot during the next time interval.

- An optimization unit that captures current and future power demands of both the PEVs and the regular electric loads over a specific time interval: The proposed optimization unit solves a two-stage optimization problem in order to determine its charging/discharging decisions. The goal of the first stage is to reach a feasible power allocation decision for the PEVs (a target PEV SOC), while including consideration of the electric grid constraints, customer demands, and current and future system power loads. The second stage is designed to efficiently utilize available resources in order to satisfy the target PEV SOC requirements while minimizing system operating costs.
- An evaluation of the performance of the proposed architecture in a variety of scenarios, based on computer simulations: The simulation results demonstrate the superior performance of the proposed architecture relative to a first-come, first-served (FCFS) benchmark.

The remainder of the paper is organized as follows. A review of related work is provided in Section II; the proposed system architecture is described in Section III; and the prediction and optimization units of the proposed architecture are explained in Sections IV and V, respectively. Section VI presents sample case studies, and Section VII summarizes the conclusions.

II. Related Work

The literature includes reports of a number of studies related to the problem of coordinated PEV charging and discharging in a smart grid. This work can be divided into two categories of solutions: The first includes myopic solutions, in which the charging and discharging decisions are based solely on the current information in the grid [7] - [11]. The second category includes forecast-based solutions, in which future power demands in the grid are considered during the determination of the charging and discharging decisions [13] - [20].

In [7], a real-time coordinated PEV charging strategy is proposed, which takes into account the time-varying energy process and the charging time and zone preferred by the PEV owner. PEV demand side management is presented in [8], with the goal of providing dynamically configurable dispersed energy storage during peak power demand and outage conditions. An autonomous distributed vehicle-to-grid (V2G) control system is suggested in [9] as a means of satisfying the requirements for scheduled charging. In [10], the development of a framework is for V2G ancillary service modeling and operation is described. An optimal PEV charging model that responds to the time-of-use price in a regulated market is proposed in [11]. The authors in [12] presented a new PEV battery energy management mechanism based on cloud computing networks, which reduces PEV interactions with parking lots and the grid. The energy management mechanism is useful for massive implementations of PEVs and other smart devices that require direct communication with the grid. However, the work fails to include consideration of the utility benefits and the distribution system constraints. Since the studies mentioned are based on myopic solutions, the effect of current and future PEV charging and discharging decisions on the power grid is not considered. The feasibility of such decisions is thus not guaranteed, which means that achieving the target SOC level for PEVs can jeopardize power system reliability.

In [13], a probabilistic method is proposed for the estimation of the amount of power that can be delivered from PEVs to the grid. The charging coordination strategy presented in [14] is based on solving a global problem that optimizes day-ahead charging decisions and a local problem that optimizes the real-time connection of the vehicles to the grid. In [15], the researchers introduce a PEV charging coordination methodology based on day-ahead and/or real-time markets. Another study [16] led to the development of an intelligent unit commitment model for V2G that optimizes power system costs and emissions. Stochastic unit commitment models for PEV operation with volatile wind power generation are proposed in [17] and [18]. The work described in [19] resulted in fuzzy logic controllers for managing PEV charging/discharging in real time. The authors of [20] developed a dual PEV coordination mechanism that operates on two different levels: market operation and real-time operation. While these existing studies deal with coordinated decisions based on forecast data, they fail to include a method of forecasting the PEV load and are not based on real-time measurements and short-term predictions. The system response to short-term fluctuations in PEV load has thus not yet been examined.

In general, the formulation of PEV charging/discharging coordination, as reported in the literature, is based on either single-objective or multi-objective optimization. The goal of single-objective optimization approaches is to minimize the charging cost or system losses. In the absence of appropriate coordination, consideration of the customer target SOC in the problem constraints may result in infeasible decisions during cases of extreme peak load. An additional objective is to maximize the SOC of the PEV batteries, a goal that may be achieved at the expense of higher system operating costs. In multi-objective optimization, the objective function is to balance the operating cost with customer satisfaction. However, the reality is that customer satisfaction and the reliability of the PEV charging service should instead have higher priority than the system operating cost. As well, some research fails to address power system constraints in the problem formulation (e.g., [8], [11], [14]), a deficiency that means the methods developed in these studies can guarantee neither the feasibility of the charging and discharging decisions nor customer satisfaction.

The goal of the research presented in this paper was to provide a smart real-time coordinated charging and discharging architecture for smart grids that can address the limitations mentioned above. The incorporation of short-term predictions of PEV power demands and the use of a two-stage optimization framework guarantees both the feasibility of the charging and discharging decisions and PEV customer satisfaction.

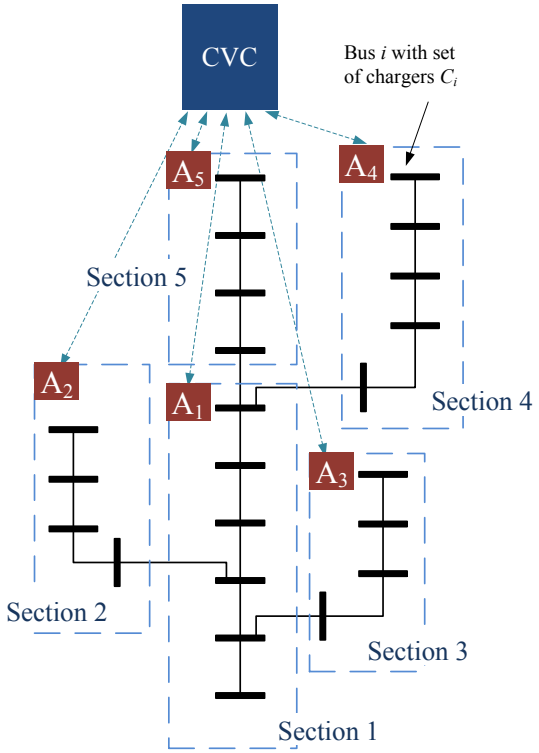

Fig. 1. Proposed SRTCS architecture.

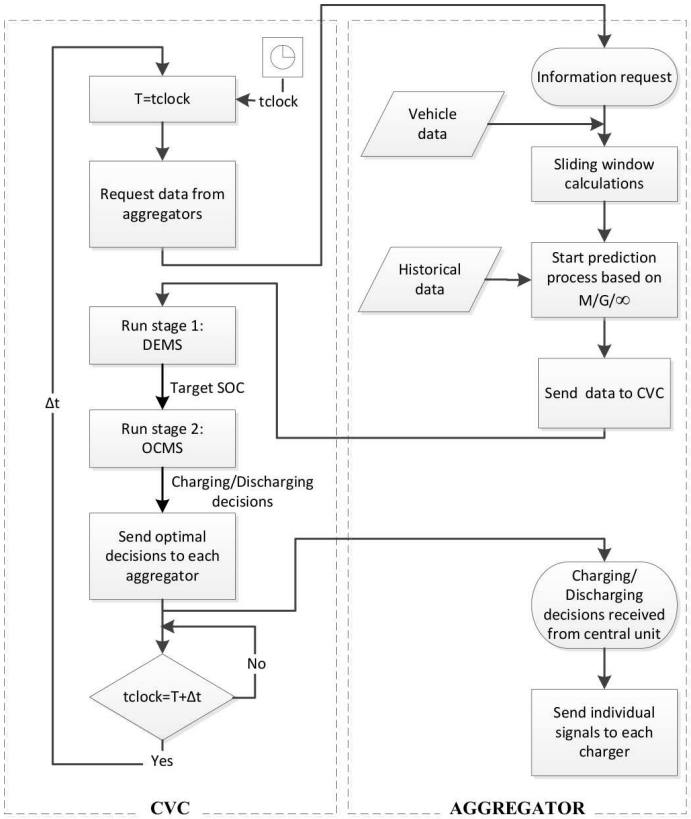

Fig. 2. Flow chart of the CVC and aggregator operation.

III. Proposed PEV Coordination Architecture

The proposed smart real-time coordination system (SRTCS) architecture is shown in Fig. 1. The smart distribution system has a set of buses $\mathcal{I}$, with each bus having a set of chargers $\mathcal{C}_i$, $i \in \mathcal{I}$. A maximum of one PEV is connected per charger. The SRTCS is also partitioned into sections, each served by one aggregator. The set of system aggregators is denoted by $\mathcal{A} = \{A_1, A_2, \ldots, A_N\}$, where N is the total number of aggregators in the system. The whole system is served by one central vehicle controller (CVC). The prediction and optimization units are located inside the aggregators and the CVC, respectively.

Each vehicle driver provides the system with the vehicle charging identity (ID), his/her parking duration, and the required SOC value, which should be less than or equal to a maximum value displayed on the charging panel.[1] The maximum SOC value depends on the battery capacity, the battery characteristics, the charger capacity, and the parking duration. The current SOC value of the PEV is also made available to the aggregator through the physical measurement of the battery pack voltage. Three types of SOC values can therefore be defined: required, maximum, and current.

The operation of the CVC and the aggregator is illustrated in Fig. 2. The aggregator receives a request for information from the CVC at a time instant t_u, $u \in \mathcal{U}$, with $\mathcal{U}$ denoting a vector that represents the CVC information request events. At t_u, the aggregator starts to process the vehicle data in all parking lots in the territory served by the aggregator. Using the processed data, the aggregator defines a prediction interval τ_{au} for each $a \in \mathcal{A}$ and $u \in \mathcal{U}$. The prediction unit forecasts the number of PEVs in the system during the prediction interval τ_{au}, which is given as the maximum parking duration of all PEVs under the jurisdiction of the aggregator $a \in \mathcal{A}$. The choice of τ_{au} ensures that the CVC has information about the PEV load in the system sufficiently far ahead to enable optimal coordination decisions to be produced. Each aggregator sends its prediction duration τ_{au} to the CVC, which defines a unified prediction interval τ_u so that all aggregators can impose a synchronous operation such that $\tau_u = \max\{\tau_{au}, a \in \mathcal{A}\}$. Given τ_u, which is sent back from the CVC, each aggregator runs its prediction unit in order to forecast the number of PEVs in the system during the next τ_u interval, interval, given the current PEV load in the system. Each aggregator then transmits to the CVC the information about currently connected PEVs along with the predicted number of PEVs. Once the CVC receives this information from all aggregators in the system, it runs its optimization unit. To produce its charging/discharging decisions, the optimization unit solves a two-stage optimization problem. The first stage is aimed at reaching a feasible power allocation decision with respect to a target SOC value for each PEV connected, while including consideration of the electric grid constraints, customer demand (SOC required by the PEV), and current and future system power loads. Future power loads include both the PEV loads predicted by the aggregators for the next τ_u interval and the

[1]The driver-required SOC value can be less than the maximum SOC value because it is dependent on the drivers preferences, the current electricity price, and his/her daily trips.

regular load forecast. The regular load forecast can follow any of the conventional techniques described in [21]. The first stage is referred to as the delivered energy maximization stage (DEMS). The second stage is designed to achieve the efficient utilization of the available resources in order to satisfy the target PEV SOC, as calculated in the DEMS, while minimizing system operating costs. The second optimization stage is referred to as the operating cost minimization stage (OCMS). The completion of this sequential structure results in charging/discharging decisions that are guaranteed to be feasible. The decisions are then transmitted from the CVC to the aggregators, which send an individual control signal to each charger under its jurisdiction. The entire process is repeated after a time duration Δt for a synchronous operation, $\Delta t \ll \tau_u$. The duration of Δt should be sufficiently long to allow for computation and communication delays.

In the following two sections, the aggregator prediction unit and the CVC optimization unit are discussed in greater detail.

IV. Aggregator PEV Prediction Unit

The aggregator PEV prediction unit predicts the number of PEVs that will be simultaneously present in the parking lots under the jurisdiction of that aggregator during the next τ_u interval.

The time is partitioned into a set of intervals $\mathcal{T} = \{T_1, T_2, \ldots, T_J\}$, where $\mathcal{T}$ covers 24 h of the day, with the duration of one interval $T_j \gg \tau_u$ for any $u \in \mathcal{U}$. The time intervals of $\mathcal{T}$ reflect temporal variations in the PEV arrival rates during the course of a day, as shown in Fig. 3, which indicates the arrival rates for typical residential parking lots, each of which serves one or more residential buildings. Within time interval $T_j \in \mathcal{T}$, PEV arrivals to the parking lots under the jurisdiction of aggregator $a \in \mathcal{A}$ are modeled as a Poisson process, with an arrival rate λ_{aj}. The durations of the PEVs' stay in the parking lot T^r_{aj} follow a general distribution with probability density function (PDF) $f_{T^r_{aj}}(t)$ and mean time $\bar{T}^r_{aj}$. The capacity of each parking lot under the jurisdiction of aggregator a is $H^{\max}_a$ PEVs.

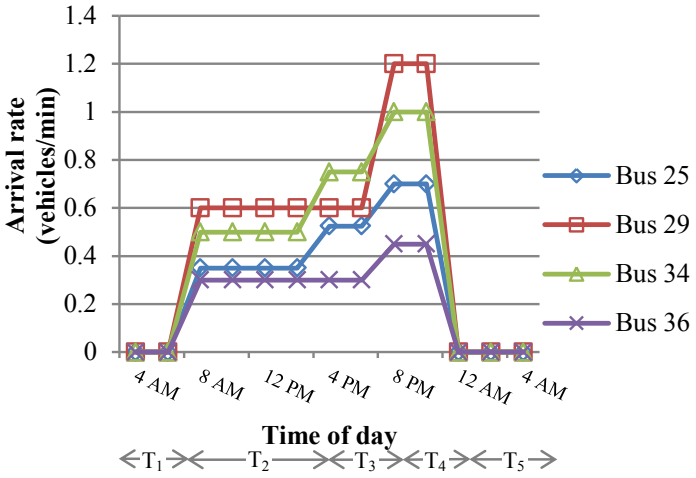

Fig. 3. Temporal variations in the PEV arrival rates.

The next operation takes place during each time interval $T_j \in \mathcal{T}$ and for each parking lot under the jurisdiction of each aggregator $a \in \mathcal{A}$. Once the aggregator receives the unified prediction interval value τ_u from the CVC, the prediction unit determines the number of PEVs that will be simultaneously present during τ_u. The prediction interval is partitioned into a set of periods $\mathcal{D}_u = \{D_{1_u}, D_{2_u}, \ldots, D_{B_u}\}$, each with an equal duration Δt, where $B_u = \lceil \frac{\tau_u}{\Delta t} \rceil$. This process is shown in Fig. 4, with the end of period D_{b_u} being denoted by t_{b_u}. Given the number of PEVs present at the time instant $H(t_u)$ and their parking durations, a simple calculation provides the number of PEVs that will stay until the end of each period in $\mathcal{D}_u$, which is denoted by $\widetilde{H}_1(t_{b_u})$. Since the PEV arrivals follow a Poisson process, the duration of each PEVs stay follows a general distribution, and since all PEVs are served without queuing, the transient analysis of an $M/G/\infty$ queuing model [22], [23] can be used to determine the number of PEVs that will arrive during $D_{b_u} \in \mathcal{D}_u$ and stay in each parking lot until the end of each period t_{b_u}. Specifically, assuming a stationary PEV arrival and departure process in T_j, PEV arrivals follow a Poisson process with a mean $\upsilon_{abu} = \lambda_{aj} \cdot b_u \cdot \Delta t \cdot q_{abu}$, where q_{abu} denotes the probability that a PEV arriving at a parking lot under the jurisdiction of aggregator a during $(t_u, t_{b_u}]$ is still present in the same parking lot at time t_{b_u}. The probability q_{abu} is given by the following [23]:

$$q_{abu} = \int_0^{b_u \cdot \Delta t} \frac{1}{b_u \cdot \Delta t} \Pr(T^r_{aj} > s) ds = \int_0^{b_u \cdot \Delta t} \frac{1}{b_u \cdot \Delta t} (1 - F_{T^r_{aj}}(s)) ds. \quad (1)$$

Hence, the predicted number of new PEV arrivals by the end of period D_{b_u}, $\widetilde{H}_2(t_{b_u})$ is given as the minimum integer that satisfies

$$\sum_{h=0}^{\widetilde{H}_2(t_{b_u})} \frac{\upsilon^h_{abu} e^{-\upsilon_{abu}}}{h!} \geq (1 - \epsilon) \quad (2)$$

where $\epsilon \in [0, 1]$ is the prediction error probability.

As a result, the predicted number of PEVs that will be simultaneously present in the parking lots under the jurisdiction of aggregator a by the end of t_{b_u} is given by $\widetilde{H}(t_{b_u}) =$

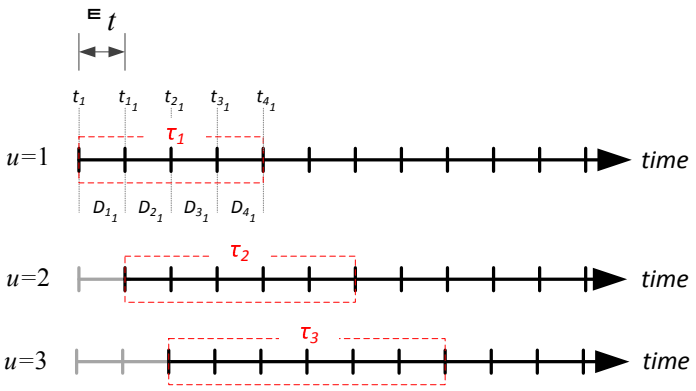

Fig. 4. Prediction intervals.

$\widetilde{H}_1(t_{b_u}) + \widetilde{H}_2(t_{b_u})$. If $\widetilde{H}(t_{b_u}) > H_a^{\max}$, then $\widetilde{H}(t_{b_u}) = H_a^{\max}$ because additional PEVs will not be admitted to the parking lot chargers . All aggregators reply to the CVC request with their prediction of the number of PEVs under their jurisdiction during the next interval τ_u.

V. CVC Optimization Unit

TThe CVC optimization unit makes coordinated charging/discharging decisions over a time duration τ_u for all chargers located under its jurisdiction. Two optimization units are proposed: the first does not allow PEV discharging, while the second does. Over the prediction interval τ_u and with consideration of the predicted PEV and regular load values, each unit solves two sequential optimization stages: DEMS and OCMS. Although the two stages provide charging/discharging decisions at every time instant t_u and t_{b_u}, during τ_u, only the decisions at time instant t_u are implemented. The decisions at the other time instants t_{b_u} during τ_u are used as initial conditions employed for the solution of the two stages for the next prediction interval τ_{u+1}, as shown in Fig. 4. The details of the operation of the optimization unit for charging only and for charging/discharging are explained in subsections A and B, respectively.

AAccording to the distribution system code developed by the Ontario Energy Board, a local distribution company may disconnect loads for the following reasons: non-payment, emergency, safety, or technical limit violation [24]. In this work, it is therefore assumed that the utility will deliver the required amount of energy to customers unless there is a technical limit violation. Hence, as a first priority, the CVC unit satisfies PEV energy requirements subject to the technical limits of the system. As a second priority, the system then minimizes operating costs.

A. Charging-Only Optimization Unit

In this case, only charging decisions are allowed. The optimization unit solves the following two stages.

1) DEMS: The objective of this stage is to maximize the energy delivered to all PEV batteries, including both those already connected and those predicted. The energy delivered at time instant $t_{(b+1)_u}$ is denoted for a PEV (actual or predicted) connected to charger $c(i) \in \mathcal{C}_i$ at bus $i \in \mathcal{I}$, due to a decision taken at time instant t_{b_u} as $E_D(c(i), t_{b_u})$. The charging decision $X(c(i), t_{b_u})$ is a percentage of the charging power permitted for charger $c(i)$ at time instant t_{b_u}, i.e., $X(c(i), t_{b_u}) \in [0, 1]$. The subset of chargers at bus i with connected PEVs (actual and predicted PEVs) is set to be $\mathcal{C}_{ip} \subset \mathcal{C}_i$. The objective of the DEMS can then be described as

$$\max_X \sum_{\mathcal{I}} \sum_{\mathcal{C}_{ip}} E_D(c(i), \tau_u) \tag{3}$$

where $X = (X(c(i), t_{b_u}) : c(i) \in \mathcal{C}_{ip}, i \in \mathcal{I}, t_{b_u} \in \mathcal{D}_u)$ and $E_D(c(i), \tau_u)$ is the energy delivered for a PEV battery at charger $c(i)$ during an interval τ_u.

The voltages and generated power levels at the system buses are specified based on the power flow constraints, where the decision variables are the voltage magnitudes and angles at all buses other than the slack bus; in addition to, the generated active and reactive powers at the slack bus. The DEMS should thus satisfy the power flow constraints, as given by

$$P_G(i, t_{b_u}) - P_L(i, t_{b_u}) = \sum_{i' \in \mathcal{I}} \{V(i, t_{b_u}) V(i', t_{b_u}) \\ Y(i, i') \cos(\theta(i, i') + \delta(i', t_{b_u}) - \delta(i, t_{b_u}))\}, \ \forall i \in \mathcal{I}, b, u \tag{4}$$

$$Q_G(i, t_{b_u}) - Q_L(i, t_{b_u}) = -\sum_{i' \in \mathcal{I}} \{V(i, t_{b_u}) V(i', t_{b_u}) \\ Y(i, i') \sin(\theta(i, i') + \delta(i', t_{b_u}) - \delta(i, t_{b_u}))\}, \ \forall i \in \mathcal{I}, b, u \tag{5}$$

where $P_G(i, t_{b_u})$ and $Q_G(i, t_{b_u})$ denote the per unit active and reactive power generated at bus i for time insta t_{b_u}, $P_L(i, t_{b_u})$ and $Q_L(i, t_{b_u})$ denote the per unit active and reactive power demands, $V(i, t_{b_u})$ and $\delta(i, t_{b_u})$ denote the per unit magnitude and angle of the voltage, and $Y(i, i')$ and $\theta(i, i')$ are the per unit magnitude and angle of the Y-bus matrix admittance.

The voltage limits and thermal limits of the feeders should also hold, i.e.,

$$V_{\min} \leq V(i, t_{b_u}) \leq V_{\max}, \quad \forall i \in \mathcal{I}, b, u \tag{6}$$

$$|I(i, i', t_{b_u})| \leq I_{\max}(i, i'), \quad \forall i, i' \in \mathcal{I}, b, u \tag{7}$$

where $I(i, i', t_{b_u})$ denotes the per unit current through the line between buses i and i'.

The power generated at each bus is obtained from the DG connected to that bus, with the exception of bus 1, which is connected to the main substation:

$$P_G(i, t_{b_u}) = P_{DG}(i, t_{b_u}), Q_G(i, t_{b_u}) = Q_{DG}(i, t_{b_u}), \\ \forall i \in \mathcal{I} \setminus \mathcal{I}_s, b, u \tag{8}$$

where $P_{DG}(i, t_{b_u})$ and $Q_{DG}(i, t_{b_u})$ denote the per unit DG active and reactive power levels generated at bus i for time instant t_{b_u}, which is based on current measurements and forecasted data, and $\mathcal{I}_s$ is the set containing the slack bus.

The total active power consumed by load $P_L(i, t_{b_u})$ is the sum of the power consumed by the regular load $P_{RL}(i, t_{b_u})$ and the PEV load $P_{PEV}(i, t_{b_u})$:

$$P_L(i, t_{b_u}) = P_{RL}(i, t_{b_u}) + P_{PEV}(i, t_{b_u}), \quad \forall i \in \mathcal{I}, b, u. \tag{9}$$

The power consumed at each bus due to the PEV load is dependent on the charging decision $X(c(i), t_{b_u})$, the chargers power limit transferred to/from the battery in kW $P_{CH}(c(i), t_{b_u})$, and the efficiency of the charger $\eta_{CH}(i)$, as given by

$$P_{PEV}(i, t_{b_u}) = \sum_{\mathcal{C}_{ip}} \frac{X(c(i), t_{b_u}) \cdot P_{CH}(c(i), t_{b_u})}{\eta_{CH}(i) \cdot K}, \\ \forall i \in \mathcal{I}, b, u \tag{10}$$

where K is the base power for the per unit system in kW. The chargers power transfer limit $P_{CH}(c(i), t_{b_u})$ is a function of the PEV battery SOC and is limited by the capacity of the charger. This function is dependent on the characteristics of

the battery:

$$P_{CH}(c(i),t_{b_u}) = f_{CH}^{c(i),t_{b_u}}(S_F(c(i),t_{b_u})), \quad \forall i \in \mathcal{I}, b, u \tag{11}$$

where $f_{CH}^{c(i),t_{b_u}}(\cdot)$ is a function that represents the characteristics of the PEV battery connected to charger $c(i)$ at bus i and time t_{b_u}, and $S_F(c(i),t_{b_u})$ is the SOC achieved at time instant $t_{(b+1)_u}$ for a PEV connected to charger $c(i) \in \mathcal{C}_i$ at bus $i \in \mathcal{I}$, due to a decision taken at time t_{b_u}. The relationship between the energy delivered to a PEV battery and the battery SOC is expressed as

$$E_D(c(i),\tau_u) = E_B(c(i)) \sum_b \{S_F(c(i),t_{b_u}) - S_0(c(i))\}, \quad \forall i \in \mathcal{I}, u. \tag{12}$$

where $E_B(c(i))$ is the battery capacity in kWh of the vehicle connected to charger $c(i)$ at bus i, and $S_0(c(i))$ denotes the initial SOC of the PEV at charger $c(i)$.

The SOC of the connected PEVs should be limited by the SOC desired by the user $S_D(c(i),t_{b_u})$:

$$S_F(c(i),t_{b_u}) \le S_D(c(i),t_{b_u}), \quad \forall i \in \mathcal{I}, b, u. \tag{13}$$

On the other hand, the predicted incoming PEVs are assumed to require a final SOC of 100% and to arrive with a minimum SOC of $S_{\min}$, which represents the worst case condition:

$$S_0(c(i)) = S_{\min}, S_D(c(i)) = 100\%, \forall c(i) \in \mathcal{C}_{ir}, i \in \mathcal{I} \tag{14}$$

where $\mathcal{C}_{ir} \subset \mathcal{C}_i$ denotes the set of chargers reserved for the newly arrived PEVs.

The SOC values for different PEVs are updated according to

$$S_F(c(i),t_{(b+1)_u}) = S_F(c(i),t_{b_u}) + \frac{X(c(i),t_{b_u}) P_{CH}(c(i),t_{b_u}) \frac{\Delta t}{60}}{E_B(c(i))}, \quad \forall i \in \mathcal{I}, 1 \le b \le B-1, u. \tag{15}$$

The DEMS is thus given by

$$\begin{aligned} \max_X \quad & \sum_{\mathcal{I}} \sum_{\mathcal{C}_{ip}} E_D(c(i),\tau_u) \\ s.t. \quad & (4)-(15) \\ & X \in [0,1]. \end{aligned} \tag{16}$$

2) OCMS: Based on the charging decisions X, a feasible target SOC $S_R(c(i))$ can be calculated for each PEV, given the power system constraints and the SOC required by the customers. The target SOC will be the same as the customer-desired SOC as long as it does not violate the technical constraints of the system. The OCMS is designed to find alternative charging decisions X that can satisfy the feasible target SOC $S_R(c(i))$ and the system power constraints, while at the same time minimizing system operating costs. During time interval τ_u, the operating costs consist of two parts: the cost of losses $C_L(\tau_u)$ and the peak demand charges $C_P(\tau_u)$. The cost of losses is given by

$$C_L(\tau_u) = \sum_b c_e(t_{b_u}) \cdot K \cdot P_s(t_{b_u}) \cdot \frac{\Delta t}{60} \tag{17}$$

where $c_e(t_{b_u})$ is the price signal, which represents the cost of kWh during interval t_{b_u}, and $P_s(t_{b_u})$ is the system power loss, given by

$$P_s(t_{b_u}) = \frac{1}{2} \sum_i \sum_{i'} G(i,i') \{V^2(i,t_{b_u}) + V^2(i',t_{b_u}) - 2V^2(i,t_{b_u})V^2(i',t_{b_u}) \cos(\delta(i',t) - \delta(i,t))\}, \quad \forall b, u \tag{18}$$

where $G(i,i')$ is the per unit conductance of the line between buses i and i'. TThe peak demand charges are calculated based on the peak load reached within one month, but the SRTCS operates in real time over time interval τ_u. To incorporate the peak demand charges $C_P(\tau_u)$ within the SRTCS, a target peak value $\widetilde{P}_{\max}(\tau_u)$ is used as in [25], which is updated to the maximum total load power incurred during τ_u, $P_{\max}(\tau_u)$, but only if this maximum power exceeds $\widetilde{P}_{\max}(\tau_u)$:

$$\widetilde{P}_{\max}(\tau_u) = \max\{\widetilde{P}_{\max}(\tau_{u-1}), P_{\max}(\tau_{u-1})\}. \tag{19}$$

The OCMS minimizes the peak demand charges only if the maximum power incurred during τ_u is greater than the target peak value:

$$C_P(\tau_u) = c_d \cdot K \cdot (P_{\max}(\tau_u) - \widetilde{P}_{\max}(\tau_u)), \quad P_{\max}(\tau_u) > \widetilde{P}_{\max}(\tau_u); \tag{20}$$

otherwise, $C_P(\tau_u) = 0$, where c_d denotes the peak demand charges in \$/kW. By definition,

$$P_{\max}(\tau_u) = \max_b \{\sum_{i \in \mathcal{I}} P_L(i,t_{b_u})\}. \tag{21}$$

The OCMS is hence given by

$$\begin{aligned} \min_X \quad & C_L(\tau_u) + C_P(\tau_u) \\ s.t. \quad & (4)-(7),(14),(15),(21) \\ & S_F(c(i),\tau_u) = S_R(c(i)) \\ & X \in [0,1]. \end{aligned} \tag{22}$$

B. Charging/Discharging Optimization Unit

In this case, discharging decisions are allowed. However, charging/discharging decisions are not implemented unless the charging-only decisions cannot satisfy the customer needs. In other words, decisions from the charging-only unit are checked first, and if they satisfy all of the customers needs (100% success), the charging decision is implemented. If the charging decisions cannot achieve 100% success, the charging/discharging unit is enabled, and its results are implemented only if they would achieve greater success than those produced by the charging-only unit. The charging/discharging optimization unit has the same structure as the charging-only one, including the objective functions and constraints of the DEMS and OCMS, with the exception of constraints (10) and (11), and the X range, as discussed next.

Since discharging is permitted, $X \in [-1,1]$, in which positive decisions denote charging and negative ones indicate

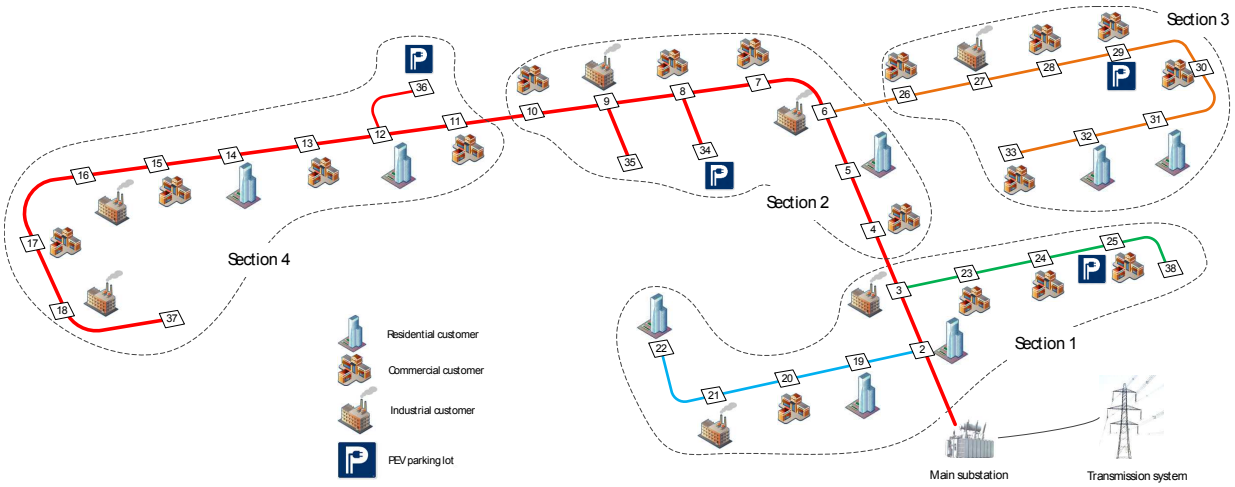

Fig. 5. 38-bus distribution test feeder.

discharging. The power delivered or consumed by each charger is given by

$$P_o(c(i),t_{b_u}) = \frac{X(c(i),t_{b_u}) \cdot P_{CH}(c(i),t_{b_u})}{\eta_{CH}(i) \cdot K}, \quad \forall X(c(i),t_{b_u}) \geq 0 \tag{23}$$

$$P_o(c(i),t_{b_u}) = \frac{X(c(i),t_{b_u}) \cdot P_{CH}(c(i),t_{b_u}) \cdot \eta_{CH}(i)}{K}, \quad \forall X(c(i),t_{b_u}) < 0. \tag{24}$$

The total power delivered by each parking lot is given by

$$P_{PEV}(i,t_{b_u}) = \sum_{c_{ip}} P_o(c(i),t_{b_u}), \qquad \forall i \in \mathcal{I}, b, u. \tag{25}$$

The power transfer limit of the charger $P_{CH}(c(i),t_{b_u})$ has different characteristics for charging and discharging:

$$P_{CH}(c(i),t_{b_u}) = f_{CH}^{c(i),t_{b_u}}(S_f(c(i),t_{b_u})), \quad \forall X(c(i),t_{b_u}) \geq 0 \tag{26}$$

$$P_{CH}(c(i),t_{b_u}) = f_{DCH}^{c(i),t_{b_u}}(S_f(c(i),t_{b_u})), \quad \forall X(c(i),t_{b_u}) < 0. \tag{27}$$

The charging/discharging optimization unit uses discharging only to increase the success rate of the PEV charging through a vehicle-to-vehicle (V2V) scheme; i.e., no power is delivered to the grid. Hence, we have

$$P_{PEV}(i,t_{b_u}) \geq 0, \qquad \forall i \in \mathcal{I}, b, u \tag{28}$$

to ensure that power is exchanged only among PEVs within the same parking lot; i.e., no power is delivered to the grid.[2]

To ensure that whenever the vehicle owner unplugs his/her PEV before the declared departure time the SOC is not less than its initial value, the discharging scheme should satisfy the following constraint:

$$S_F(c(i),t_{b_u}) \geq S_0(c(i)), \qquad \forall i \in \mathcal{I}, b, u. \tag{29}$$

[2]For a V2G scheme, this constraint is removed from the SRTCS.

VI. Simulation Results and Discussion

To evaluate the performance of the proposed SRTCS, two case studies were examined using a 38-bus system [26] that contains a mix of residential, commercial, and industrial customers and PEV parking lots, all of which are supplied from the main power substation, as shown in Fig. 5. The total system peak load is 4.37 MVA. The system line data, customer type, and load point demand are as given in [26]. The system under study, including aggregators and prediction units, was modeled in a MATLAB software tool. The CVC optimization unit was modeled in a General Algebraic Modeling System (GAMS) software tool. To update the SOC of the PEV batteries, charging/discharging decisions are sent from the GAMS to the MATLAB environment. For the simulation, $\Delta t = 10$ min, and the simulation covers 24 h of one day. The maximum computation times for the prediction and optimization units in the system under study are 1.1 sec and 75 sec, respectively. The hardware utilized for simulation was a quad core 2.8 GHz processor with 6 GB of RAM. The error probability for the prediction unit is $\epsilon = 0.1$. The peak demand charge is 3 \$/kW [27], and the energy cost is as shown in Fig. 6. The initial moving peak value for the day under study is set to the maximum regular load demand: 3.715 MW.

The system contains four parking lots on buses 22, 29, 34, and 36, as shown in Fig. 5. The PEV parking residence time is modeled in the prediction unit as an exponential random variable with mean times of 120 min, 180 min, 120 min, and 100 min for the four parking lots, respectively. For simplicity, all chargers are assumed to be second-level chargers with a 7.2 kW rating. All PEVs are assumed to have an all-electric range (AER) of 50 miles. All PEV batteries have the same charging/discharging characteristics, as given in [29] with some adjustment to the match the ratings of the PEV chargers and the AER. For simplicity, the function representing

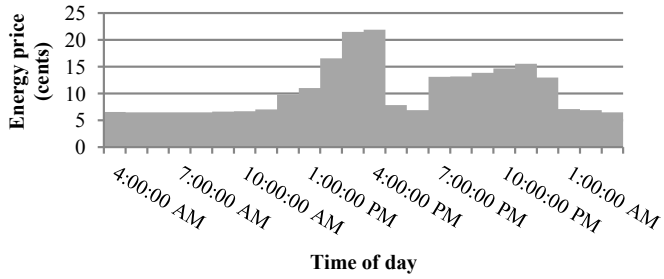

Fig. 6. Real-time energy price.

the battery characteristics in (11), which is included in the Appendix, is assumed to be identical for all vehicles.

Two case studies were examined. The first investigated the performance of the SRTCS with charging-only (SRTCS-C) decisions for a low PEV penetration level. The second case study evaluated the performance of the SRTCS for a high PEV penetration level with both charging-only and charging/discharging (SRTCS-C/D) decisions. In both cases, the proposed SRTCS was compared to an FCFS approach for coordinated charging decisions [28]. In the FCFS approach, PEV charging decisions are based on allocating priority to vehicles that arrive at the parking lot earlier. The SRTCS was also compared to an uncoordinated charging approach, whereby all PEVs connected to the grid are charged without consideration of the technical limitations of the system and in the absence of communication between the grid operators and the PEVs. A success factor SF is introduced as a figure of merit. The success factor is defined as the mean success of PEV charging for all vehicles in the system over the 24 h under study and is given by

$$SF = \frac{1}{H} \cdot \sum_{h=1}^{H} \frac{E_D(h)}{E_R(h)} \tag{30}$$

where H denotes the total number of PEVs served during the 24 h of the day, and $E_D(h)$ and $E_R(h)$ denote the energy delivered and required for PEV h, respectively.

A. Smart PEV Charging with Low PEV Penetration

In this case study, the total PEV load represents 18% of the total system load. The PEV arrival rates at the parking lots are shown in Fig. 3. The regular load of the system over the 24 h period is shown in Fig. 7(a) [30]. TThe maximum number of PEVs, i.e., chargers, in each parking lot is 25, 75, 25, and 25 for buses 25, 29, 34, 36, respectively. As shown in Fig. 7(b), both the uncoordinated (UNCR) and FCFS approaches yield the same performance, which is attributable to the low PEV penetration level, which enables the system to charge all connected PEVs without violating the technical limitations. On the other hand, the proposed SRTCS can significantly reshape the charging requirement of the PEVs connected to the system. With the use of the SRTCS, during the regular load peak, PEV charging is limited and is performed either before or after the peak load interval, thanks to the prediciton unit. In contrast to the uncoordinated and FCFS approaches, with the SRTCS, the

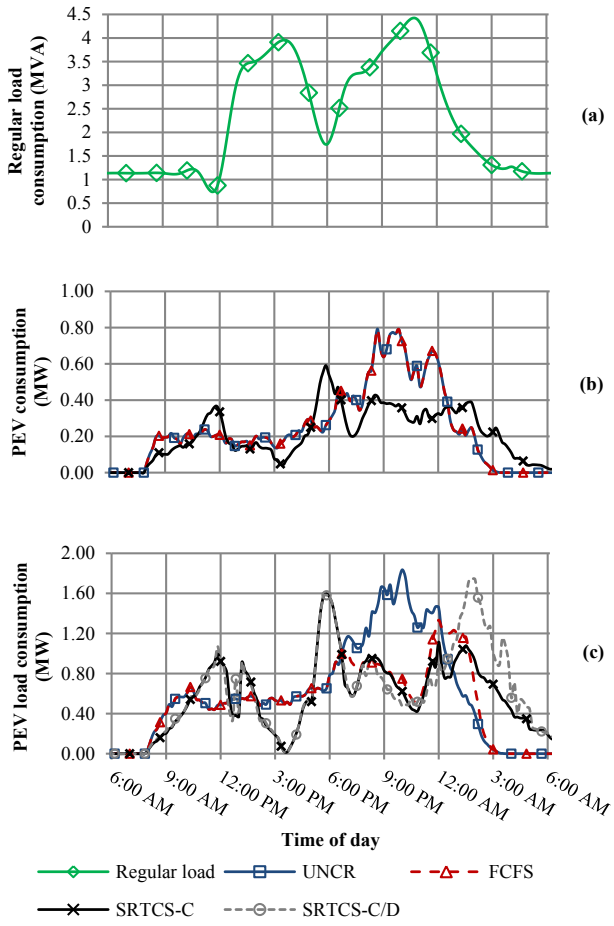

Fig. 7. Power demands for regular and PEV loads for different scenarios: (a) Regular load demand; (b) PEV demand at low penetration; and (c) PEV demand at high penetration.

TABLE I
SYSTEM OPERATING COSTS AND SUCCESS FACTORS FOR THE LOW PENETRATION CASE

Scheme	*SF* (%)	Percentage reduction in C_L(%)	Percentage reduction in C_P(%)	Feasibility
UNCR	100.0	0.0	0.0	Feasible
FCFS	100.0	0.0	0.0	Feasible
SRTCS-C	100.0	14.6	47.2	Feasible

PEV charging peaks occur at the periods of minimum regular load: around 11:30 am, 5:30 pm, and after 1 am. IWith low PEV penetration, all three charging approaches can achieve a success factor of $SF = 100\%$. Table I shows the percentage reduction in operating costs compared to the UNCR scenario. Because the PEV charging energy is allocated during low price periods, the SRTCS results in a significant reduction in the cost of the system losses: 14.6%. The peak demand charges for the SRTCS are also 47.2% lower due to the ability of the SRTCS to shift the peak of the PEV load to the off-peak periods of the regular load, as shown in Fig. 7(b).

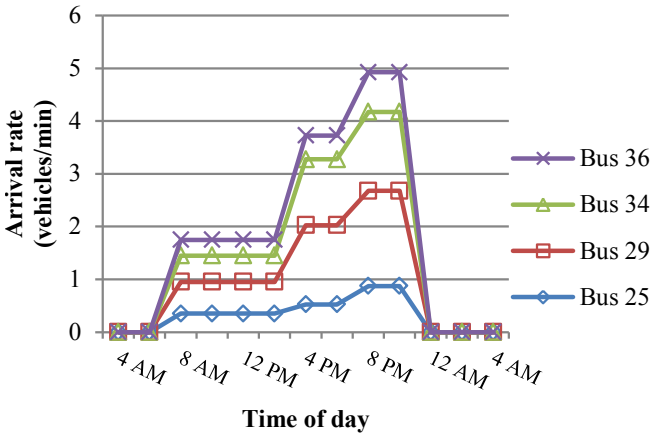

Fig. 8. PEV arrival rates for the case with a high penetration level.

TABLE II
SYSTEM OPERATING COSTS AND SUCCESS FACTORS FOR THE HIGH PENETRATION CASE

Scheme	*SF* (%)	Percentage reduction in C_L(%)	Percentage reduction in C_P(%)	Feasibility
UNCR	100.0	0.0	0.0	Infeasible
FCFS	85.7	17.7	76.0	Feasible
SRTCS-C	91.3	17.9	71.7	Feasible
SRTCS-C/D	97.7	15.9	67.1	Feasible

B. Smart PEV Charging/Discharging with High PEV Penetration

In the second case study, the PEV penetration represents 42% of the total load of the system. For uncoordinated vehicle charging, such a penetration level is beyond the technical limitations of the system. The PEV arrival rates are given in Fig. 8. The maximum number of PEVs in each parking lot is 50, 150, 50, and 50 for buses 25, 29, 34, 36, respectively. The PEV load results are shown in Fig. 7(c) and Table II. While the uncoordinated approach can achieve a success factor of $SF = 100\%$, the charging decisions are infeasible because they violate the system constraints. Using the predictions for the regular and PEV loads, the SRTCS can shift the PEV load so that a higher success factor is achieved than with the FCFS approach, at a slightly higher cost in losses and a lower peak load charge. As shown in Fig. 7(c), the SRTCS reduces the PEV load during regular load peak periods, e.g., 3:30 pm and 10:30 pm, to reduce the peak demand charges, and the PEV load also peaks during the regular load off-peak periods, as in the previous case.

The results demonstrate that the SRTCS is more reliable than the other approaches with respect to addressing the PEV charging requirements through the efficient utilization of system resources. The SRTCS achieves a significantly higher success factor of 97.7% when discharging is enabled, which successfully shifted the peak PEV consumption to regular load off-peak periods, as shown in Fig. 7(c). However, this result is obtained at the expense of a higher operating cost than in the charging-only case. The higher cost with respect to losses is due to excess charging energy, which correlates with the higher success factor. On the other hand, the higher peak demand in the case of enabled discharging compared with the charging-only case is due to the change in load pattern that occurs immediately after the operation of the discharging unit. An examination of Fig. 9 offers an explanation of this effect. The discharging unit is activated at 7:40 pm due to the failure of the charging unit to deliver the energy required. Once the discharging unit is activated, some of the vehicle energy is discharged and transferred to other vehicles in the same parking lot, with the goal of maximizing the entire amount of energy delivered to the PEVs within the time interval under study. This process results in equal or higher loading on the system after 7:40 pm in the discharging case compared with the situation in the charging-only case because the discharged PEVs will be transferred to become part of the demand at a later time instant after 7:40 pm. This shift can then create a higher total peak demand in the system at the trough shown in Fig. 7(c), which occurs at 10:30 pm.

However, according to utility regulations [24], from the operators' point of view, the service reliability of the PEV charging (in terms of the success factor) is considered a higher priority than the operating costs. The charging schemes can be compared by assuming an individual success factor $SF_n(h)$=$E_R(h)/E_D(h)$, where $0\% < SF_n(h) < 100\%$. The entire range of the $SF_no(h)$ is divided into 7 levels, as shown in Table III. As indicated, with the SRTCS-C/D scheme, in the entire 24 h period, only 1.4% of the PEVs, representing a total required charging energy of 125.6 kWh, left the parking lots without receiving any charge. On the other hand, with the charging-only scheme, 6.39% of the PEVs, representing a total required charging energy of 755.7 kWh, left the parking lot without receiving any charge. These values are much higher with the FCFS charging scheme. Most of the vehicles are plugged in for short periods (10 min to 1 h) during the peak period from 7:40 pm to 11:30 pm. For a 100% individual success factor, when the discharging unit was enabled, 96.41% of the PEVs received the charging energy they required, for a total of $14,514.5$ kWh, while only 87.33% and 80.53% of the PEVs were fully satisfied in the charging-only and FCFS cases, respectively.

VII. CONCLUSIONS AND FUTURE WORK

This paper has presented a proposed real-time system for managing the dynamics associated with coordinated charging/discharging decisions for PEVs in a smart grid. The SRTCS incorporates two novel prediction and optimization units. For better coordination of vehicle charging, the prediction unit provides information regarding the future PEV load in the system. The two-stage optimization unit guarantees the feasibility of the charging/discharging decisions by first maximizing PEV owner satisfaction and then minimizing system operating costs. The performance of the SRTCS has been investigated for both low and high PEV penetration levels and for charging-only and charging/discharging decisions. The simulation results demonstrate the robust performance of the

TABLE III
DETAILS OF THE INDIVIDUAL SUCCESS FACTORS FOR THE HIGH PENETRATION LEVEL

	Percentage of served PEVs (%)			Required energy (kWh)			Delivered energy (kWh)		
	FCFS	SRTCS-C	SRTCS-C/D	FCFS	SRTCS-C	SRTCS-C/D	FCFS	SRTCS-C	SRTCS-C/D
SF°=0%	11.20	6.39	1.40	1304.4	755.7	125.6	0.0	0.0	0.0
0% < SF°≤ 20%	0.58	0.51	0.31	148.8	119.2	57.2	25.5	12.1	3.9
20% < SF°≤ 40%	2.39	1.23	0.55	473.1	254.2	115.4	159.4	73.7	29.9
40% < SF°≤ 60%	2.73	1.20	0.61	579.2	243.8	103.9	299.1	121.5	53.1
60% < SF°≤ 80%	1.64	1.81	0.51	340.8	407.9	99.7	233.0	293.2	68.6
80% < SF°< 100%	0.92	1.30	0.20	167.9	242.9	43.8	151.0	217.7	42.3
SF° =100%	80.53	87.33	96.41	12044.5	13034.0	14514.5	12044.5	13034.0	14514.5

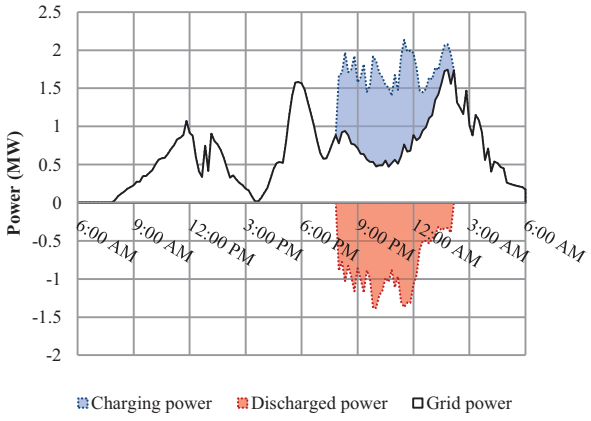

Fig. 9. Detailed illustration of the performance of the SRTCS-C/D for a high penetration level.

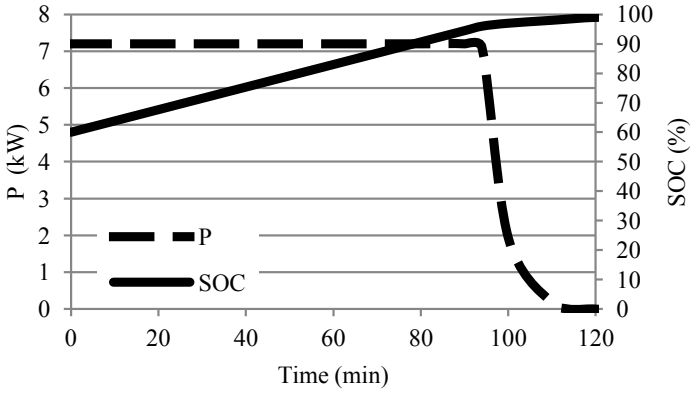

Fig. 10. Li-ion battery characteristics.

proposed SRTCS with respect to its ability to address the dynamics of multiple parking lots in a timely manner. The findings also reveal the effectiveness of the SRTCS architecture in providing a higher PEV charging success rate than other charging approaches. The advantages of the proposed SRTCS can thus be summarized as providing immunity to extreme loading conditions, robustness, and an acceptable computation time, all of which make it suitable for practical implementation.

Although the discharging operation results in an improved SOC for the PEVs, a number of related technical issues present challenges, such as its unknown impact on battery life and the requirement for PEV manufacturers to agree to include such an operation in their design. Future research should thus include the investigation of appropriate compensation for PEV owners who adopt such a strategy. Compensation that is too low would discourage them from embracing the discharging strategy, while compensation that is too high would motivate utilities to deploy other options such as DG or storage devices. The establishment of an appropriate compensation value that balances the benefits for both PEV owners and utilities needs further study.

APPENDIX

Fig. 10 rrepresents the charging characteristics of a typical PEV Li-ion battery pack [29]. The charging characteristics consist of two regions: a constant-current charging phase and a constant-voltage phase, in which the charging power decays gradually, as shown, in order to avoid battery overcharging.

REFERENCES

[1] D. Wu, D. Aliprantis, and K. Gkritza, "Electric energy and power consumption by light-duty plug-in electric vehicles," *IEEE Trans. Power Systems*, vol. 26, no. 2, pp. 738-746, May 2011.
[2] R. Liu, L. Dow, and E. Liu, "A Survey of PEV Impacts on Electric Utilities," in *Proc. ISGT'11*, pp. 1-8, Oct. 2011.
[3] M. F. Shaaban, Y. M. Atwa, and E. F. El-Saadany, "PEVs modeling and impacts mitigation in distribution networks," *IEEE Trans. Power Systems*, Early access, 2013.
[4] H. Khayyam, H. Ranjbarzadeh, and V. Marano, "Intelligent control of vehicle to grid power," *J. Power Sources*, vol. 201, pp. 1-9, March 2012.

[5] R. A. Verzijlbergh, M. O. W. Grond, Z. Lukszo, J. G. Slootweg, and M. D. Ilic, "Network impacts and cost savings of controlled EV charging," *IEEE Trans. Smart Grid*, vol. 3, no. 3, pp. 1203-1212, Sept. 2012.

[6] O. Sundstrom and C. Binding, "Flexible charging optimization for electric vehicles considering distribution grid constraints," *IEEE Trans. Smart Grid*, vol. 3, no. 1, pp. 26-37, March 2012.

[7] S. Deilami, A. S. Masoum, P. S. Moses, and M. A. S. Masoum, "Real-time coordination of plug-in electric vehicle charging in smart grids to minimize power losses and improve voltage profile," *IEEE Trans. Smart Grid*, vol. 2, no. 3, pp. 456-467, Sept. 2011.

[8] C. Pang, P. Dutta, and M. Kezunovic, "BEVs/PHEVs as dispersed energy storage for V2B uses in the smart grid," *IEEE Trans. Smart Grid*, vol. 3, no. 1, pp. 473-482, March 2012.

[9] Y. Ota, H. Taniguchi, T. Nakajima, K. M. Liyanage, and J. Baba, "Autonomous distributed V2G (vehicle-to-grid) satisfying scheduled charging," *IEEE Trans. Smart Grid*, vol. 3, no. 1, pp. 559-564, March 2012.

[10] C. Quinn, D. Zimmerle, and T. H. Bradley, "An evaluation of state-of-charge limitations and actuation signal energy content on plug-in hybrid electric vehicle, vehicle-to-grid reliability, and economics," *IEEE Trans. Smart Grid*, vol. 3, no. 1, pp. 483-491, March 2012.

[11] Y. Cao, S. Tang, C. Li, P. Zhang, Y. Tan, Z. Zhang, and J. Li, "An optimized EV charging model considering TOU price and SOC curve," *IEEE Trans. Smart Grid*, vol. 3, no. 1, pp. 388-393, March 2012.

[12] H. Khayyam, J. Abawajy, B. Javadi, A. Goscinski, A. Stojcevski, and A. Bab-Hadiashar, "Intelligent battery energy management and control for vehicle-to-grid via cloud computing network," *Applied Energy*, vol. 111, pp. 971-981, Nov. 2013.

[13] S. Han, S. Han, and K. Sezaki, "Estimation of achievable power capacity from plug-in electric vehicles for V2G frequency regulation: case studies for market participation," *IEEE Trans. Smart Grid*, vol. 2, no. 4, pp. 632-641, Dec. 2011.

[14] Y. He, B. Venkatesh, and L. Guan, "Optimal scheduling for charging and discharging of electric vehicles," *IEEE Trans. Smart Grid*, vol. 2, no. 3, pp. 1095-1105, Sept. 2012.

[15] R. J. Bessa, M. A. Matos, F. J. Soares, and J. A. P. Lopes, "Optimized bidding of a EV aggregation agent in the electricity market," *IEEE Trans. Smart Grid*, vol. 3, no. 1, pp. 443-452, March 2012.

[16] A. Y. Saber and G. K. Venayagamoorthy, "Intelligent unit commitment with vehicle-to-grid - A cost-emission optimization," *J. Power Sources*, vol. 195, no. 3, pp. 898-911, Feb. 2010.

[17] M. E. Khodayar, L. Wu, and M. Shahidehpour, "Hourly coordination of electric vehicle operation and volatile wind power generation in SCUC," *IEEE Trans. Smart Grid*, vol. 3, no. 3, pp. 1271-1279, Sept. 2012.

[18] C. Liu, J. Wang, A. Botterud, Y. Zhou, and A. Vyas, "Assessment of impacts of PHEV charging patterns on wind-thermal scheduling by stochastic unit commitment," *IEEE Trans. Smart Grid*, vol. 3, no. 2, pp. 675-683, June 2012.

[19] M. Singh, K. Thirugnanam, P. Kumar, and I. Kar, "Real-time coordination of electric vehicles to support the grid at the distribution substation level," *IEEE Systems Journal*, to appear.

[20] K. De Craemer, S. Vandael, B. Claessens, and G. Deconinck, "An Event-Driven Dual Coordination Mechanism for Demand Side Management of PHEVs," *IEEE Trans. Smart Grid*, to appear.

[21] I. S. Moghram and S. Rahman, "Analysis and evaluation of five short-term load forecasting techniques," *IEEE Trans. Power Systems*, vol.4, no.4, pp.1484-1491, Nov. 1989.

[22] D. Gross, J. F. Shortle, J. M. Thompson and C. .M. Harris, *Fundamentals of Queueing Theory*, Wiley series in probability and statistics, Aug. 2008.

[23] M. R. H. Mandjes and P. Zuraniewski, "M/G/infinity transience, and its applications to overload detection," *Performance Evaluation*, vol. 68, no. 6, pp. 507-527, Feb. 2011.

[24] Ontario energy board, "Distribution system code," June 2013, available online: http://www.ontarioenergyboard.ca/OEB/_Documents/Regulatory/Distribution_System_Code.pdf.

[25] T. Logenthiran, D. Srinivasan, and T. Z. Shun, "Demand Side Management in Smart Grid Using Heuristic Optimization," *IEEE Trans. Smart Grid*, vol. 3, no. 3, pp.1244-1252, Sept. 2012.

[26] D. Singh, R. Misra, and D. Singh, "Effect of load models in distributed generation planning," *IEEE Trans. Power Systems*, vol. 22, no. 4, pp. 2204-2212, Nov. 2007.

[27] Avialable online: http://www.hydroone.com/RegulatoryAffairs/RatesPrices/Pages/SmallBusinessDeliveryRates.aspx.

[28] J. Huang, V. Gupta, and Y-F. Huang, "Scheduling algorithms for PHEV charging in shared parking lots," in *Proc. IEEE ACC'12*, pp. 276-281, June 2007.

[29] F. Marra, G. Y. Yang, C. Trholt, E. Larsen, C. N. Rasmussen, S. You, "Demand profile study of battery electric vehicle under different charging options," in *Proc. IEEE PES GM'12*, pp. 1-7, July 2012.

[30] E. Lopez, H. Opazo, L. Garcia, and P. Bastard, "Online reconfiguration considering variability demand: applications to real networks," *IEEE Trans. Power Systems*, vol.19, no.1, pp.549-553, Feb. 2004.